Earthquake Engineering, Tenth World Conference © 1992 Balkema, Rotterdam. ISBN 90 5410 060 5

A study on the Cypress Viaduct collapse and seismic performance of a retrofitted bent

H.Ohuchi, T.Matsuda & Y.Goto
Technical Research Institute, Obayashi Co., Tokyo, Japan

ABSTRACT: This paper describes numerical simulation studies on the bent collapse of the Cypress Viaduct during the Loma Prieta Earthquake and on the seismic performance of the same type bent retrofitted. The purpose of the 1st simulation is to identify seismic behavior of collapsed and survived bents due to ground condition and structural types and that of 2nd simulation is to estimate seismic performance against several earthquakes consistent with the current U.S. design standard. Nonlinear dynamic response analyses provided quantitative explanation on the relationship between ground conditions, bent types and bent collapses and also ensured sufficient seismic safety of the retrofitted bent.

1. Introduction

The cause of the Cypress Viaduct bent damages in the 1989 Loma Prieta Earthquake is considered as deeply related with the underlying ground condition and the structure type. The Cypress north side section was on reclaimed soft soil, while the south side section on dense silty sand. In the north side, all the upper decks fell down onto lower decks except one span portion. On the other hand in the south side falling down of upper decks was prevented except about 150m portion next to the north side.

The bent types are conceptually categolized into 3 structure types as shown in Fig.1. B type bent was employed in many parts and all collapsed in the north side. Among five A type bents existed in the north side, two of them survived despite significant damages suffered. In the south end of north side, all the C type bents also collapsed.

Present numerical simulations are classified into two phases, i.e. collapse simulation of existed bents and seismic performance simulation of a retrofitted bent.

The objective of 1st simulation is to provide rational answer to the following two questions: Are bent collapse in the north side section and bent survival in the south side section predicted if considering different ground conditions? and do B and C type bents collapse and an A type bent not collapse in the north side section?

Analytical studies for this simulation consist of 4 parts: 1)Dynamic response analysis of ground, 2)Soil-foundation dynamic interaction analysis, 3)Static non-linear analysis of bent and 4)Nonlinear dynamic response analysis of bent based on parts 1) to 3) results.

The objective of 2nd simulation is to provide similar rational answer to the following question: How much structural margin does retrofitted bent possess against earthquakes with acceleration amplitude consistent with the current seismic design standard? Analytical studies for this simulation consist of two parts : 5)Static nonlinear analysis and 6)Nonlinear dynamic response analysis of retrofitted bent. Results from parts 1) and 2) analyses are also utilized as an input motion and foundation characteristics for the part 6)dynamic response analysis.

It should be noted that all the above analyses are carried out against lateral motion neglecting structural contribution from the longitudinal members except their gravity load.

2. Collapse Simulations

2.1 Dynamic Response of Ground

A dynamic response analysis of a multilayered ground is conducted based on the

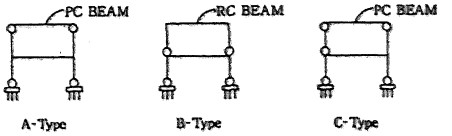

Fig.1 Bent type - conceptual structure.

multiple reflection theory. An equivalent linearization method is utilized to consider nonlinear behavior of soil materials. Soil layers in the north side and south side sections are modelled on the basis of boring log datas and PS velocity logging datas by Caltrans(1990). An accelerogram recorded at Yerba Buena Island, rocky outcrop about 7 km distant from the Cypress section (EW : 0.067G, NS : 0.029G) is employed as an input wave from bedrock. A half of EW component, is utilized as the incident wave from bedrock.

Fig.2 illustrates the calculated transfer function between bedrock and ground surface, in which the amplification in the higher frequency region is larger in the north side than in the south side. The analytical period agrees fairly well with the measured value of 0.7Hz in the ambient vibration by Ohmachi(1989). Fig.3 illustrates the calculated ground surface acceleration waves. In these analyses, the attained maximum shear strain of each layer is in the range of 6.5×10^{-5} to 9.4×10^{-5}.

2.2 Soil-Foundation Dynamic Interaction

As a pair of bent columns stand on the independent foundation with each other, a unit of pile cap - foundation system is idealized. Representative analytical bents to be discussed in this paper are No.96, 85 and 71 for A, B and C type bent respectively. An asymmetric dynamic response analysis is conducted with using axsymmetric finite elements. The material characteristics of ground layers such as shear stiffness and damping are modelled based on the results in the previous ground response analysis.

The horizontal stiffness of the spring which corresponds to the ground model and the effective input acceleration on the top of pile cap are evaluated for the later three degrees of freedom system model shown in Fig. 10. Fig.4 illustrates frequency dependent characteristics of the spring analytically obtained. The real part corresponds to stiffness while the imaginary part damping characteristic.

The effective input motion which is required to take the kinematic interaction into account, is shown in Fig.5. It is calculated with using input of the prescribed earthquake wave from the virtual bedrock.

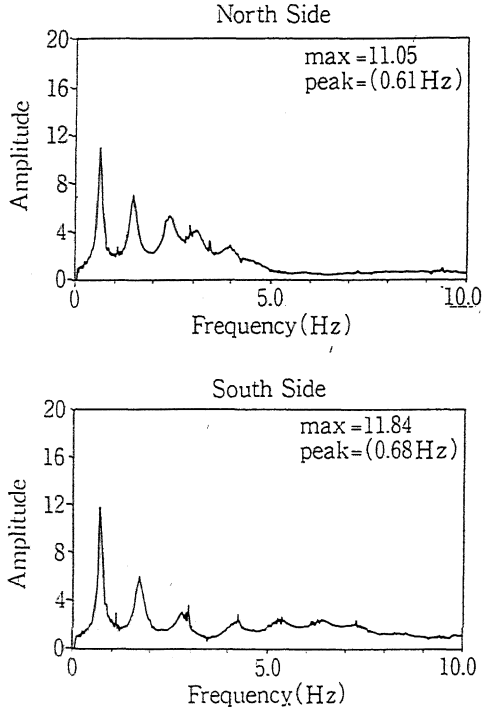

Fig.2 Transfer function between bedrock and ground surface.

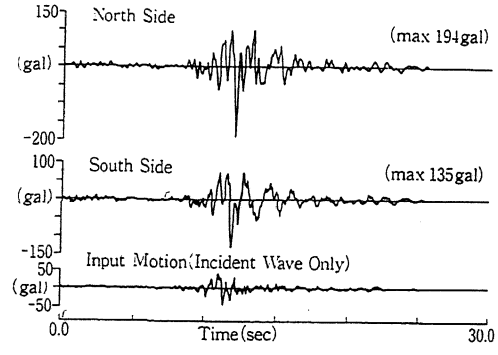

Fig.3 Ground surface acceleration based on multiple reflection theory.

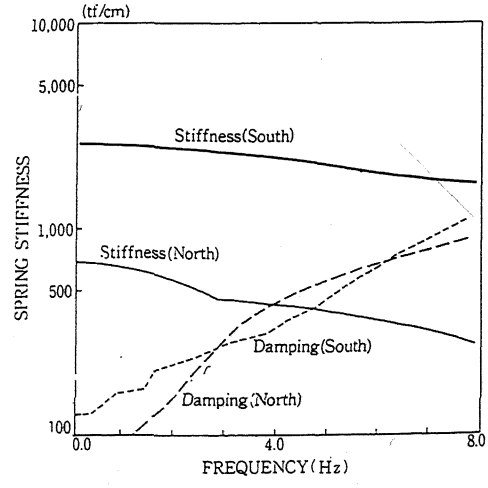

Fig.4 Frequency dependent characteristics of spring.

2.3 Static Nonlinear Behavior of Bents

The objectives in this section are to predict bent type dependent critical failures and load-displacement relationships for the nonlinear dynamic response analysis in the following section.

Material constants for two dimensional finite element nonlinear analyses are assumed on the basis of design informations and sampling test results by Moehle(1990).

After applying dead load, i.e. weight of bent caps and one span length box girder, static horizontal load uniformly distributed in each bent cap is increased. The load ratio between upper and lower stories is determined by the elastic first mode.

These analytical results predict flexural yielding failure for A type bent and shear failure for B and C type bents. In the B type bent, after the joint shear cracks extend to the concrete coverage, most of shear reinforcement in the pedestal ultimately yield. In the C type bent with pinned joints at both upper column tops, the shear crack initiates from pedestal to joint at relatively high horizontal load. However, because one of upper columns resists no horizontal load, the lateral shear force concentrates on the other column, resulting in lower ultimate loading capacity and lower lateral stiffness obtained rather than the B type bent.

The ultimate loading capacity of the B or C type bent is numerically determined by the load level when the internal lateral shear force in the critical column rapidly decrease umbalancing with the external horizontal load.

A typical bent failure sequence observed in the field investigation by Nims(1989) is illustrated in Fig.6. A predicted ultimate crack pattern of B type bent is comparatively shown in Fig.7. Even during dead load application, the shear crack initiates in the pedestal below the pinned joint of upper column due to shear force outward the joints. With horizontal load increasing, this crack propagates diagonally along bent down rebar in the joint and then vertically into concrete outer-coverage, which corresponds the failure mode illustrared in Fig.6. The left end of upper bent cap is critical in flexural crack shown as the broken line in Fig.7, which suggests a flexural crack concentration at upper bent cap end as shown in Fig.6 when considerng insufficient anchorage effect of #18 lower straight reinforcement and bond depression under cyclic horizontal load. Fig.8 illustrates predicted horizontal strain contour at ultimate stage.

It is effective to describe accuracy of the present analysis in comparison with the nondestructive field test result conducted

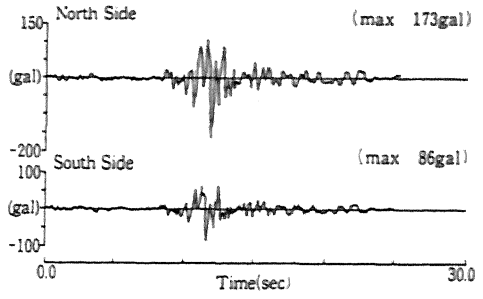

Fig.5 Effective ground surface acceleration.

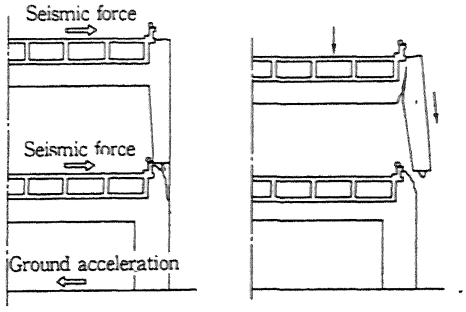

Fig.6 Typical failure sequence of B type bent.

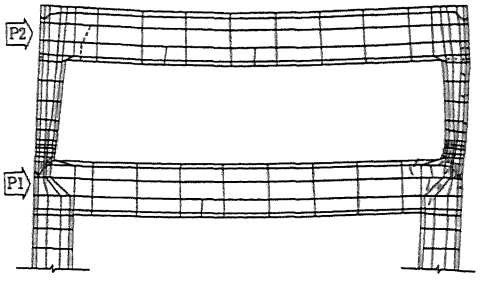

Fig.7 Ultimate crack pattern of B type bent.

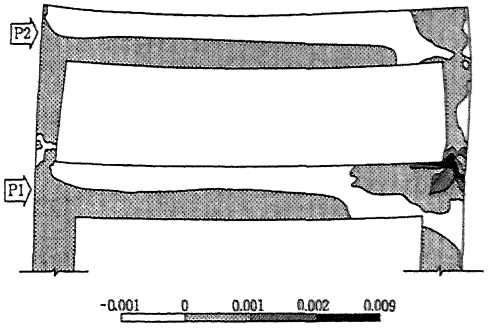

Fig.8 Horizontal strain ε_x contour of B type bent at ultimate stage.

by Moehle(1990). Fig.9 illustrates analytical and experimental load-displacement relationships, where the analytical result agrees with experimental result in the ascending part with some difference in ultimate loading capacity, i.e. 156tf for analysis and 210tf for experiment. This difference is due to the concrete tensile strength leading shear failure of bents with much less shear reinforcement.

2.4 Nonlinear Dynamic Response of Bents

Nonlinear dynamic response analyses are conducted with using three degrees of freedom systems taking soil-foundatin interaction effect into account as shown in Fig.10. As for the enveloping curve of hysteresis models, shear force-relative displacements obtained from the finite element nonlinear analyses are idealized into tri-linear model. As for the hysteretic rule, the flexural-failure-type degrading stiffness response model is utilized for both upper and lower stories of the A type bent. In the B and C type bents, similar model is utilized for the lower story while the origin-orient hysteresis model for the upper story critical in brittle shear. Based on the dynamic interaction analysis in the previous section, the spring characteristcs at base is idealized as a linear elastic model with damping calculated considering strain energy for radiation damping. Superstructure damping is assumed as of 3 %.

The obtained acceleration time histories and shear force - relative displacement hystresis in the critical upper story are tabulated in Table.1 in which characteristic responses can be identified due to bent types and ground conditions. In the north side B and C type bents, the upper story collapses immeadiately after the maximum ground surface acceleration. On the other hand in the south side, both type bents survive with some stiffness reduction appearance. The A type bent in the north side does not collapse with hysteretic damping effect due to flexural yielding. This analytical performance ensures survival of actual No.95 and No.96 bents despite considerable damages observed.

3. Seismic Performance Simulation of Retrofitted Bents

3.1 Static Nonlinear Behavior of Retrofitted Bents

Moehle(1990) conducted horizontal loading tests of retrofitted bents using survived No.45 to No.47 bents with less damages. First of all, comparison with this destruct-

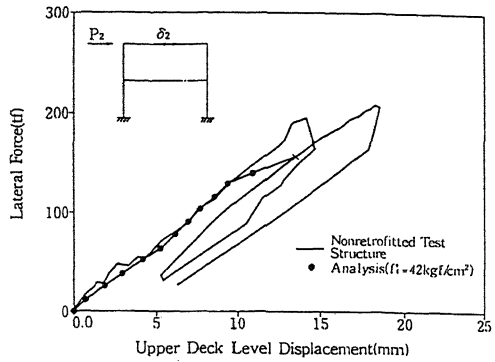

Fig.9 Load-displacement relationship of No.46 bent.

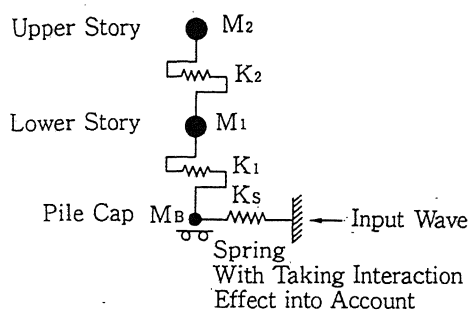

Fig.10 Three degrees of freedom system model for nonlinear dynamic response.

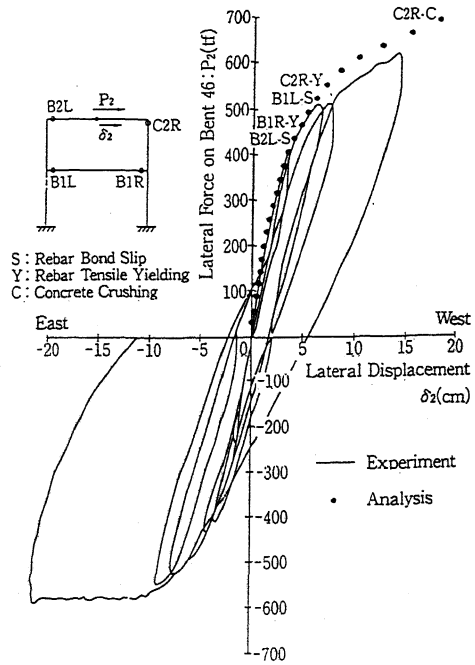

Fig.11 Load-displacement relationship of retrofitted No.46 bent.

Table 1 Bent responses dependent on bent types and ground conditions.

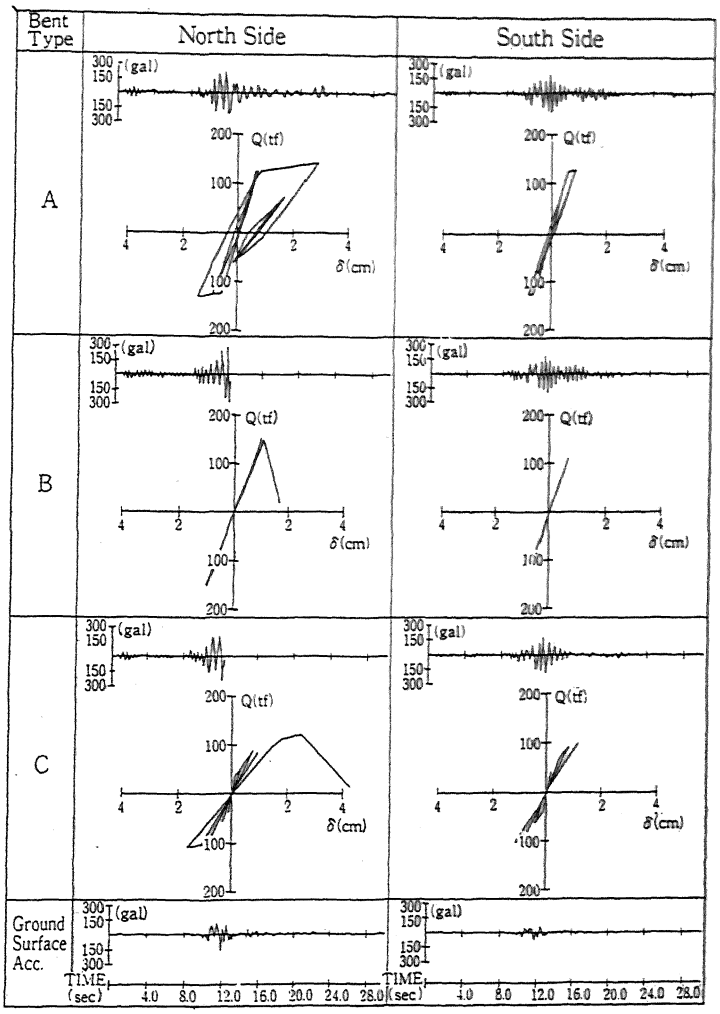

ive test with load application only at upper story should be conducted to verify the accuracy. The retrofitted No.46 bent, presently categorized as B type bent is analyzed in this chapter.

Inadequate and insufficient anchorage effect of the bent cap lower reinforcement should be considered. Insufficient anchorage directed depression is modelled by reducing yielding strength of #18 rebar in the joints based on the pull-out test results referenced by Park(1975).

A comparison between experimental and analytical load-displacement relationship is shown in Fig.11 to represent good approximation of a finite element nonlinear analysis ensuring flexural type failure.

In the next step, the similar bent under horizontal loads both at upper and lower stories is analyzed for the later dynamic response analysis. This result provides that the locations of yield hinges produced are completely same as former one, despite they appear in about 10% earlier load stage.

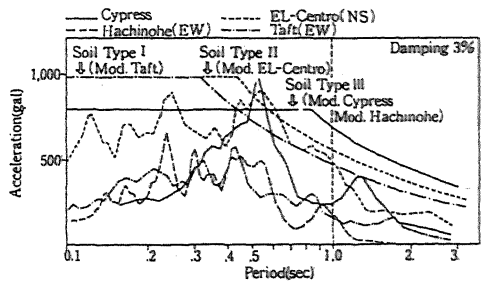

Fig.12 Elastic acceleration spectrums.

3.2 Design Response Spectrum and Input Motion

Fig.12 illustrates elastic acceleration response spectrums by the previously predicted acceleration wave on the Cypress north side with the representative acceleration records in the past. The elastic seismic response spectrums for three soil types specified in the ATC Code(1986) are also shown. Design response fitted waves are respectively produced for three soil types by modifying acceleration amplitude of these waves with its phase angle unchanged.

3.3 Nonlinear Dynamic Response of Retrofitted Bents

A three degrees of freedom system is modelled for the Cypress wave and the modified Cypress wave, while a two degrees of freedom system for another three modified waves because foundation and ground conditions are not identified. The flexural failure type degrading stiffness model is also idealized for both upper and lower hysteresis characteristics.

For the original Cypress wave, both upper and lower story responses remain in elastic. Except this case, the shear force reaches beyond elastic limit but not beyond yielding for any cases. The maximum response and the seismic performance evaluation in strength and ductility are provided in Table.2 for each input motion respectively, where the ultimate strength and the ultimate displacement are temporarily defined by the yielding shear force Q_y and the relative displacement δ_u when concrete crush initiates at the upper story column top respectively. For all input waves, sufficient safety factor is assured in both strength and ductility.

4. Concluding Remarks

Based on the results presented, a number of conclusions can be summarized as follows:

1) Two dimensional finite element analysis predicted nonlinear behaviors of the existed bents and of the retrofitted bent up to the failure with good agreements in comparison with experimental results.
2) The multi degrees of freedom system nonlinear response analysis, on the basis of systematized analyses, i.e. on the amplified ground motion, on the soil-foundation interaction and on the nonlinear behavior of the bents up to the ultimate, provided rational explanation for the sequential collapse scenario of the Cypress Viaduct.
3) The present type of retrofitted bent mainly in shear provides sufficient seismic performance against input motions with acceleration amplitude consistent with the current seismic design guideline.

References

Applied Technology Council, 1986. Seismic Design Guideline for Highway Bridges, 2nd Printing.

Caltrans, 1990. Log of Test Boring Concerning Cypress Viaduct.

Caltrans, 1990. Borehole Velocity Surveys at the Embarcadero in San Francisco and the Cypress Structure in Oakland.

Moehle, J.P. and Mahin, S.A. 1990. Implications Nondestructive and Destructive Tests on the Cypress Street Viaduct Structure. 7th US-Japan Workshop on Bridge Structure. UJNR.

Nims, D.K. et al. 1989. Collapse of the Cypress Street Viaduct as a Result of the Loma Priea Earthquake. UCB/EERC. 89/16.

Ohmachi T, et al. 1989. Ground Motion Characteristics in the San Francisco Bay Area Detected by Microtremor Measurements - A Preliminary Assesments. Tokyo Institut of Technology. No.800104.

Park,R. and Paulay,T. 1975. Reinforced Concrete Structures. John Wiley & Sons: 407-410.

Table 2 Seismic performance of retrofitted bent.

Input Earthquake	Story	Input		Response			Safety Factor	
		$\ddot{y}_{max}$ Max. Vel. (cm/sec)	$\ddot{y}_{max}$ Max. Acc. (gal)	$(\ddot{y}_0+\ddot{\delta})_{max}$ Max. Acc. (gal)	δ_{max} Max. Disp (cm)	Q_{max} Max. Shear Force(tf)	Q_u/Q_{max} Strength	δ_u/δ_{max} Ductility
Cypress	2	24	173	398	1.00	222	2.23	16.30
	1			221	0.51	352	2.13	---
M.Cypress	2	68	345	635	2.33	349	1.42	7.00
	1			397	1.28	527	1.42	---
M.Hachinohe	2	49	310	680	2.84	383	1.29	5.74
	1			481	1.75	567	1.32	---
M.EL-Centro	2	47	383	810	3.65	437	1.13	4.47
	1			685	1.80	571	1.31	---
M. Taft	2	52	386	729	3.04	396	1.25	5.36
	1			491	1.52	547	1.37	---